Accurate Detection and Localization of Curved Checkerboard-Like Marker Based on Quadratic Form

Shaoan Wang, Mingzhu Zhu, Yaoqing Hu, Dongyue Li, Fusong Yuan, and Junzhi Yu, *Fellow, IEEE*

***Abstract*—Checkerboard-like markers are widely applied in visual localization applications including SLAM, augmented reality, robot navigation, and 3D scene reconstruction. Most corner detectors assume that the marker is attached to a flat surface, which severely limits the placement of the marker and thus reduces the scope of use for these applications. However, in some scenarios, it is not easy to find an ideal flat surface required by most corner detectors in a given scenario, in which case the marker can often only be fixed on a curved surface. Therefore, the accuracy of most corner detectors may be reduced. In this study, a novel method is proposed with subpixel accuracy to detect and locate the corners on a chessboard-like marker which is either flat or curved. The proposed method fits multi-segment curves in quadratic form to the edges in a checkerboard-like marker. The exact corner positions are considered as the intersections of the corresponding curves with analytical solutions. The proposed method achieves state-of-the-art performance through experiments including synthetic corner localization test, real-world stereo vision triangulation experiment, and pose estimation on a curved object, demonstrating the superiority of our method.**

***Index Terms*—Corner localization, curved marker, multi-segment curve, quadratic form, subpixel precision.**

I. Introduction

VISUAL localization is a key technique for many applications such as robot navigation and augmented reality (AR) [1]–[5]. There are two mainstreams to address these applications. One is to extract natural features that exist in the environment [6]. While more convenient from a practical point of view, natural features are not guaranteed to be abundant in every scene, limiting the detection and localization feasibility. Besides, a fiducial marker that contains many easily detectable features is commonly introduced for applications with high precision requirements [7]. Furthermore, a checkerboard-like marker [8], [9] with a large number of handcrafted corner features is frequently utilized [10]. Several corner detection methods for checkerboard-like markers have been proposed in recent years, significantly facilitating the use of the checkerboard-like marker.

Existing corner detection methods [11], [12] primarily focus on planar markers and perform poorly on non-planar surfaces. In practice, when detecting the corners of checkerboard-like markers attached to curved surfaces, these methods often yield high localization errors and are not well suited to the needs of high-precision localization, such as in oral surgery. Therefore, it is difficult to apply these methods well in applications with very narrow or rugged environments. For instance, fiducial markers fixed on planar walls or ground can offer sufficient features for robots to position themselves. However, for applications where there are scenarios with narrow spaces or uneven surfaces, such as robot in-pipe navigation, a flat surface is not always available. Markers mounted on an object can also be used to provide 6D pose information of the object. However, for objects with uneven surfaces, the markers can only be placed on the object precariously, causing great inconvenience or even failure during pose estimation. For augmented reality, existing projection mapping techniques are limited to flat or quasi-flat surfaces due to the precision of corner detection methods. It will be greatly beneficial if the projection mapping techniques are available for non-flat surfaces, which requires a non-planar corner detection method. To summarize, developing a corner detection method for checkerboard-like markers on curved surfaces is both necessary and urgent.

In this paper, a novel corner detection method with subpixel accuracy is presented. Firstly, we use a two-stage filter based on image gradient and corner template to select all candidate corners precisely. Following that, the corner array is organized using a Delaunay triangulation procedure. Next, the sets of edge sampling points are extracted using the Sigmoid function. Then, we fit multi-segment curves in quadratic form to the edges of the curved checkerboard-like marker. Finally, an analytical solution of the curve intersections is introduced as the precise corner position. Experiments demonstrate the precision and robustness of the proposed method. The main contributions can be elaborated in the following two folds.

1) To improve the corner positioning accuracy of the curved checkerboard-like marker, a novel corner detection and localization method based on quadratic form is proposed. First, a two-stage corner detector that balances efficiency and accuracy is designed. Next, using the property that the quadratic form remains quadratic or

This work was supported in part by the National Key Research and Development Program of China under Grant 2020YFB1312800, in part by the National Natural Science Foundation of China under Grant 62003007, and in part by the Fundamental Research Funds for the Central Universities. *(Corresponding author: Junzhi Yu.)*

S. Wang, Y. Hu, D. Li, and J. Yu are with the State Key Laboratory for Turbulence and Complex Systems, Department of Advanced Manufacturing and Robotics, College of Engineering, Peking University, Beijing 100871, China (e-mail: wangshaoan@stu.pku.edu.cn; 2101111894@stu.pku.edu.cn; 2001111648@stu.pku.edu.cn; junzhi.yu@ia.ac.cn).

M. Zhu is with the Department of Mechanical Engineering, Fuzhou University, Fuzhou 350000, China (e-mail: mzz@fzu.edu.cn).

F. Yuan is with the National Engineering Laboratory for Digital and Material Technology of Stomatology, Center of Digital Dentistry, Peking University School and Hospital of Stomatology, Beijing 100190, China (e-mail: yuanfusong@bjmu.edu.cn).

degenerates to a line under projective transformation, multi-segment curves in quadratic form are fitted to the curved marker edges and the intersection of the curves is utilized as the precise subpixel corner position. Further, the simulation experiments demonstrate that the accuracy of the proposed method is significantly improved compared to the existing methods.

2) A new pose estimation system for objects on curved surfaces is developed by utilizing the proposed method. The performance of detection and localization is reliably verified through a series of experiments.

The remainder of this paper is organized as follows. Section II describes the literature survey on existing corner detection methods. In Section III, the details of the proposed method to extract corner positions with subpixel accuracy on curved markers are described. In Section IV, a series of experiments are carried out to evaluate the performance of the proposed method and a curved object pose estimation procedure is demonstrated to verify the feasibility of the proposed method. At last, the conclusion and future work of this paper are offered in Section V.

II. Related Work

Checkerboard-like marker detection is usually divided into two gradual stages: corner detection and subpixel refinement. Corner detection identifies all correct corner pixels and eliminates incorrect candidates as much as possible, while subpixel refinement is responsible for obtaining the subpixel coordinates of all corners. The following contents are related works on these two tasks respectively.

A. Corner Detection

Harris corner detector [11] is based on the intensity of the sliding mask centered on corners, which will change greatly no matter what the sliding direction is. However, it is difficult to rule out false positives. As another commonly used corner detector, FAST [13] compares the intensity of each pixel with neighboring pixels in the sampling circle, which leads to serious misjudgment problems as well. Using a sampling circle idea similar to FAST, Bennett and Lasenby proposed a corner detector named ChESS [12]. The key idea is to figure out if the intensity along the sampling circle is cosine-distributed or not. However, the cosine distribution is unreasonable under camera projective transformation. Zhang and Xiong [14] proposed a hypothesis that the distribution is a two-period square wave to solve this problem.

The above assumption cannot work well when the marker is attached to a curved surface or suffers severe distortion. In this case, a better option is to employ the changing pattern of pixel intensity. Sun *et al.* [15] and Yan *et al.* [16] calculated the average of the pixels on each sampling circle and binarized the sampling results. They then picked out pixels with alternating and symmetric transition points. However, it is still a difficult problem to set the proper radius under different image scales. To tackle this issue, Sun *et al.* used a set of sampling circles with different radii; a corner is confirmed only if most of the circles give a reasonable result. Although most of the black and white stripes can be filtered out, the finer stripes are still retained. That is to say, the trade-off between the width of the stripe and the radius of the sampling circle is inevitable.

Template matching has attracted plenty of attention because of its robustness to noise, perspective transformation, and lens distortion. Geiger *et al.* [17] used template matching in final corner detection. The mean shift algorithm is introduced to find two gradient directions of each candidate, based on which they calculated the correlation between the candidates and the generated corner templates to select the true corners. Yan *et al.* [16] also proposed an online template detection method, which finds the gradient direction based on four transition points and then constructs a pixel intensity template. Template matching has two main advantages. First of all, it can significantly eliminate the problem of misjudgment, and there will be no other circumstances to pass this test. Secondly, the correlation score is independent of the pixel intensity, so it is robust to illumination change. However, both the online generation and the pixel-by-pixel matching procedures of template matching consume a lot of resources, which usually means that it is hard to utilize this method on real-time tasks.

B. Subpixel Refinement

There are two mainstreams for subpixel refinement based on the corner model. The first method considered a corner as a saddle point [18], [19], whose neighborhood area can be interpreted as a surface that can be fitted by a quadratic function. For corners, the quadratic function turns out to be a hyperbolic paraboloid whose critical point, is referred to as the saddle point. Furthermore, Plachet *et al.* [20] discovered that establishing a cone-shape low pass filter as a preprocessing step can increase localization accuracy compared to the traditional normalized Gaussian filter. However, there is some curvature in the corner edges on the surface relative to the standard corner model, resulting in a slight drift in the true corner position compared to the saddle point.

Another method is intuitive that the vector from a corner to its adjacent area pixel point should be perpendicular to the gradient of the adjacent area, leading to an optimization problem that is straightforward to solve in closed form [21]. This well-known idea is utilized in many classical methods like the function *cornerSubPix* in OpenCV and Geiger *et al.* [17]. However, like some of the other methods mentioned above, the sizing of the neighborhood is an issue. Larger neighborhood sizes are affected by curved surfaces and do not meet the above assumptions, while smaller neighborhood sizes tend to amplify the effect of noise on image gradients.

Moreover, some other methods were proposed as well. Chen and Zhang [22] proposed a subpixel corner detector that directly used the Hessian matrix instead of fitting polynomials, which greatly reduced the amount of calculation but made the positioning accuracy more susceptible to external influences. Datta *et al.* [23] proposed an iterative corner refinement procedure by performing undistortion and unprojection of corners to a canonical fronto-parallel plane, which intuitively cannot utilize on a curved surface.

Corner detection and subpixel refinement are both vital to checkerboard-like marker detection. Corner detection ensures

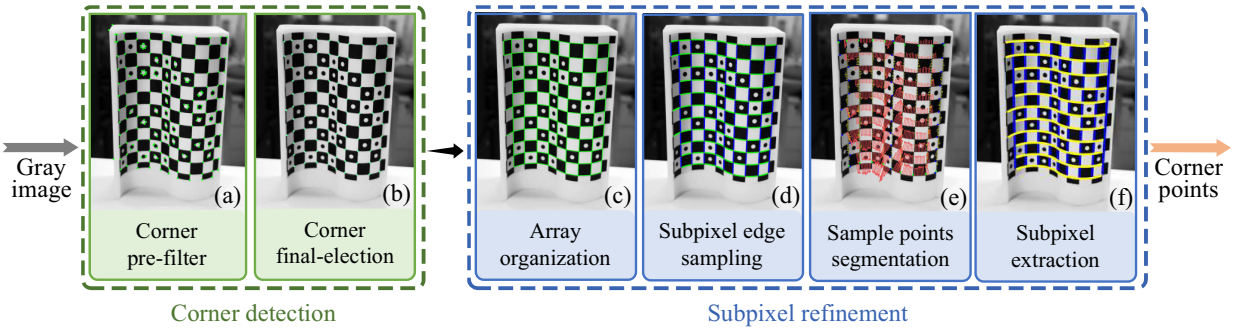

Fig. 1. Detection pipeline. The proposed method is divided into six sub-sections. (a) Fast primary selection of candidates. (b) Robust corner screening based on template matching. (c) Obtain the connected array by performing Delauney triangulation on the extracted corners. (d) Fitting sub-pixel edge sampling points based on the connected array. (e) Implement continuity-based sample point segmentation using the proposed ANCF. (f) Extract subpixel corner positions by fitting multi-segment elliptic curves and finding the intersections.

that all corners are selected out, while subpixel refinement determines the precision of the corner position. Apparently, the latter is more important to the accuracy of visual localization. Hence, the proposed method to improve the corner position accuracy with subpixel is explained in the following sections in detail.

III. Methodology

In this section, a novel corner detection method that selects all the correct candidate corners in pixel using a two-stage procedure is described. Then we organize the corners into arrays with the connectivity. Finally, a subpixel corner extraction process based on quadratic form is established to obtain the precision location of each corner. Fig. 1 illustrates the detection pipeline. The details of these steps are discussed in the following section.

A. Corner Pre-Filter

Traditional corner detectors like Harris or Shi-Tomasi [24] are common choices for this task. However, we discovered that the technique described by Chen and Zhang [22] is more resilient and efficient in terms of image blurring, large noise, and scale change when employing an image Hessian matrix. Haralick *et al.* [25] have analyzed that the eigenvalues of the Hessian matrix can represent the maximum and minimum second directional derivatives of the surface and their associated eigenvectors should be orthogonal to each other. Therefore, a new scoring function using the Hessian matrix is created. First, a low pass filter is necessary for image processing, which can reduce the effect of noise and smooth the intensity distribution around the corners. The image gradient $\boldsymbol{G} \in \mathbb{R}^2$ is then computed at each pixel p using a two-dimensional Gaussian smoothing filter with a predetermined hyperparameter σ. The Hessian matrix is calculated in each pixel similarly to Chen's method.

$$H = \begin{bmatrix} \boldsymbol{G}_{xx} & \boldsymbol{G}_{xy} \\ \boldsymbol{G}_{xy} & \boldsymbol{G}_{yy} \end{bmatrix} \tag{1}$$

For an ideal corner, the maximum eigenvalue λ_1 of the Hessian matrix is positive while the minimum eigenvalue λ_2 is negative, so the score function S can be designed as follows:

$$S = -\lambda_1 \cdot \lambda_2 = \boldsymbol{G}_{xy}^2 - \boldsymbol{G}_{xx}\boldsymbol{G}_{yy} \tag{2}$$

Pixels with higher scores are more likely to be true corners, whereas pixels around corners tend to receive similarly high scores. An intuitive idea is to keep only the pixel with the largest score within the same corner. Therefore, a conservative non-maximum-suppression [26] (with parameters n_{nms} and τ_{nms}) is applied to suppress multiple candidate pixels under the same corner. Here, n_{nms} refers to the size of the local pixel neighborhood, and τ_{nms} refers to the dimension of the non-maximum-suppression. It is obvious that pixels closer to a corner can gain higher scores. It is worth noting that our method requires the total number of corners to be input in advance to estimate the number of candidates in the Corner Pre-Filter stage. In order to reduce the amount of computation in the Corner Final-Election stage and keep all the true corners, we sort all pixels in descending order according to their scores and keep twice the number of true corners as candidate corners based on our experience.

B. Corner Final-Election

While the Corner Pre-Filter stage allows the correct corners to be selected, conditions such as pinstripes (black or white stripes with a narrow width) can also achieve high enough scores to make it difficult to be filtered out. Therefore, a robust method to reject false candidates needs to be introduced in the Corner Final-Election stage. Given the small number of candidate corners, the template matching method is ideal for obtaining excellent filter performance without a large amount of computation. Firstly, the orientation angles of the two edges around a corner χ^* are extracted using a quadratic fitting surface $\mathcal{F}(\chi^*)$ because the slight edge angular deviation causes little influence. This can be transferred to a least squares problem:

$$\underset{\alpha,\beta,\gamma,\delta,\epsilon,\zeta}{\arg\min} \left\| \left(\alpha x^2 + \beta xy + \gamma y^2 + \delta x + \epsilon y + \zeta\right) - I(x,y) \right\|_{\Omega_{n\times n}}^2 \tag{3}$$

where $I(x,y)$ is the image intensity of each pixel, Ω refers to the neighboring area of the corner χ^*, and n means the size of the neighboring area. Besides, the quadratic surface can be approximated as two hyperplanes multiplied by each other, where the boundary of each hyperplane is an edge of the corner. The orientation angles of the edges are defined as θ_1 and θ_2, which are calculated as follows:

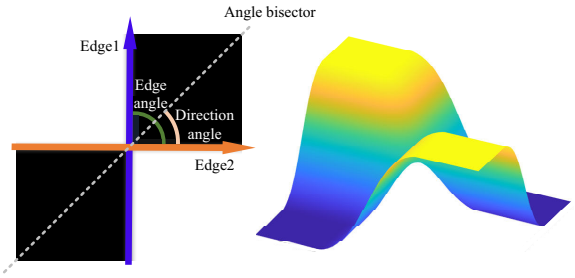

Fig. 2. A synthetic representation of a corner.

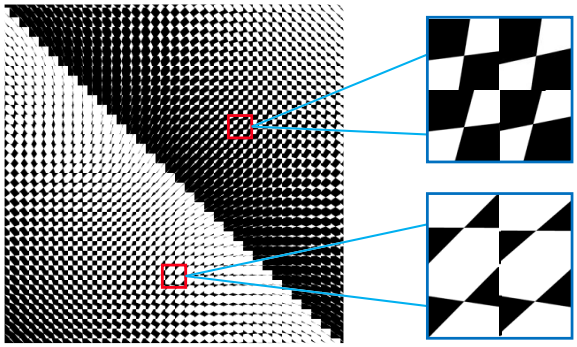

Fig. 3. The offline generated 36 × 36 corner template. For each candidate corner, a template corner with the most suitable edge angle and direction angle will be picked out to go through Corner Final-Election stage.

$$\mathcal{F}(\chi^*) \approx k(x\sin\theta_1 - y\cos\theta_1)(x\sin\theta_2 - y\cos\theta_2) + p \quad (4)$$

where $(x, y) \in \Omega_{n\times n}$. Following that, the orientation angle of each straight edge is gained and the edge angle (defined as the absolute value of the difference between two orientation angles), as well as the direction angle (defined as the angle between the angle bisector and the horizontal direction) of the candidate corner, are calculated easily.

Then, a handcrafted corner template is generated using these two angles shown in Fig. 2. Furthermore, it is also time-consuming if the template is generated online. Therefore, this paper adopts the approach of pre-generating templates offline and selecting them online to reduce the amount of computation during template generation. A problem that cannot be ignored is the number of offline templates. After a lot of simulation experiments under noise and other disturbances, we finally choose to equate the edge angle and direction angle into 36 types respectively, corresponding to a total of 36×36 cases, and generate these templates offline in Fig. 3. These two angles may range from 0° to 360° and 0° to 180°, respectively. The edge corners are divided equally into 36 cases in steps of 10° and the directional corners are divided equally into 36 cases as well in steps of 5°.

Once the orientation angles of the edges are obtained, the template with the smallest angle difference up is picked out. The response score R^*_{score} is calculated using Normalized Cross Correlation (NCC) between the neighboring area of the candidate and the template. Only if the difference between the highest response score $\max(R_{score})$ and the current response score is less than a threshold $T_{correlation}$, the candidate will be selected as a true corner.

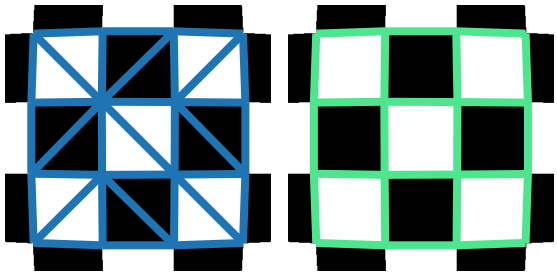

(a) (b)

Fig. 4. Delaunay triangulation presentation. (a) Original Delaunay triangulation result. (b) Connection result after removing the wrong edges.

$$R_{score} = \frac{\sum_w \sum_h (\mathcal{N} - \bar{\mathcal{N}})(\mathcal{T} - \bar{\mathcal{T}})}{\sqrt{\left(\sum_w \sum_h (\mathcal{N} - \bar{\mathcal{N}})^2\right)\left(\sum_w \sum_h (\mathcal{T} - \bar{\mathcal{T}})^2\right)}} \quad (5)$$

where $\mathcal{N}$ is the image neighboring area of the candidate corners with fixed width w and height h while $\mathcal{T}$ is the template that is picked out. As a result, all the correct corners are preserved and the wrong candidates are eliminated efficiently using this two-step filter method shown in Fig. 1(b).

C. Array Organization

In this part, the Delaunay triangulation procedure is performed for all corners extracted as described in the previous section. Delaunay triangulation is an algorithm for dividing point clouds into multiple triangles by connecting the points. The generated triangles have the property of being as obtuse as possible. It is also an efficient algorithm whose computational cost is $\mathcal{O}(n \log n)$ for n input points.

The result to obtain the connectivity among corner clusters based on Delaunay triangulation is shown in Fig. 4(a). Based on the orientation angles of the edges around the corner, the reasonable Delaunay edges are kept and all the erroneous Delaunay edges that are not close to any orientation angle are removed. Here, a threshold θ^*_{edge} to determine whether a Delaunay edge is close to the corner edge is introduced. When this process is completed for any edge, the connectivity among the corners is obtained as shown in Fig. 4(b).

D. Subpixel Edge Sampling

As the connective arrays among corners are received, it is easy to obtain the directions of the corners around one corner, which are close to related edges. Here, the corner positions and the connectivity are used to sample the edges of each corner with sub-pixel accuracy, paving the way for the following quadratic fitting part. A step function is frequently used to abstract the ideal edge model. Whereas photosensitive components are limited by the convolution effect and optical diffraction effect, there is usually a transition zone present in the practical edges shown in Fig. 5. For the practical edge,

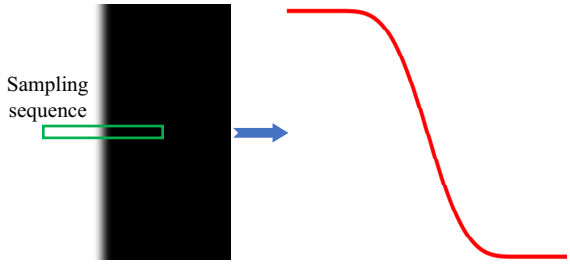

Fig. 5. Schematic of sampling on an ideal edge. The angle of the edge is perpendicular to the horizontal direction so that the direction of the sampling sequence is horizontal.

the above simulation model is more significant in the direction perpendicular to itself. However, for a discrete matrix of image pixels, it is hard to find and extract the pixels around the edge whose direction is perpendicular to it. Therefore, it is more credible and thoughtful to use neighboring pixels in the x-direction or y-direction that are closer to the vertical direction of the edge to perform the fitting method.

Subpixel edge extraction has been the classical topic of numerous studies. Considering the application scenario, the Sigmoid function is utilized to fit the practical edges:

$$Sig(\mathcal{S}) = \frac{a}{1 + e^{-(\mathcal{S} - pos_{edge})/c}} + d \tag{6}$$

where $\mathcal{S}$ is the sampling sequence. The Sigmoid function is a non-linear function that is continuous and smooth. The subpixel edge position is obtained by fitting the pixel sequence near the edges using the Sigmoid function, and the precise edge position pos_{edge} can be considered as the function position with the biggest derivative. Compared with other methods, this fitting method does not require a prior search for pixel-level edge positions, thus significantly reducing the complexity of the method.

By subpixel sampling of multiple edges around each corner, we can comprehensively consider the sampling results and the connectivity between corners to obtain the global boundary sampling results, as shown in Fig. 1(d).

E. Sampling Points Segmentation

For the general situation, we assume that the edges of the checkerboard-like markers can be represented by multiple continuous quadratic curves and straight lines since most of the curved surfaces which are commonly used can be seen as a combination of the ellipse, ellipsoid, and flat surfaces. Therefore, to obtain good fitting results, the discrete sampling points should be split into segments containing only the corresponding curves in a single plane, ellipse, or ellipsoid. However, depending on the position of the marker, the corners may be close to the surface boundary in some cases. When using a multi-vision system, if the curve is not correctly segmented, corners located at the boundaries may be shifted at different viewing angles, thus reducing positioning accuracy. Therefore, it is necessary to create a robust paradigm where all the curves and lines can be correctly separated under different viewing angles. Here, a two-stage multi-curve segmentation method is introduced.

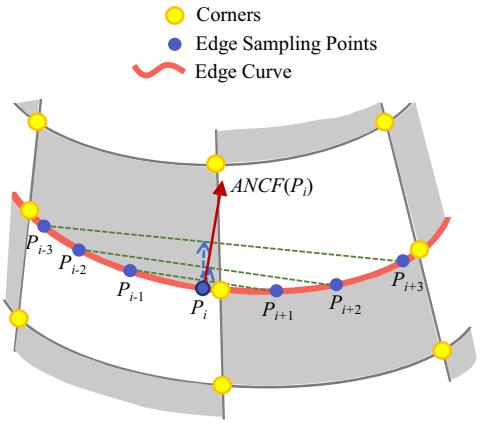

Fig. 6. A schematic of ANCF near a sampling point P_i.

The boundary between elliptic curves and lines can be mainly divided into two cases. The first is that the edge near the boundary is discontinuous, and the second is that the edge is continuous, but the direction of the normal vector near the boundary is opposite. In the first stage, we aim to pick out all sampling points with a discontinuous neighborhood edge. Based on this property, the second-order derivative near the split point should be very high with respect to the remaining points. Therefore, the absolute value of the second-order difference based on the central finite-difference approximation is used as the response score. Next, a Gaussian filter is applied to the sampling points to reduce the noise influence. It is rational that the discontinuous split points in the first case should obtain a higher score, which can easily be picked out.

For each segment obtained from the first-stage segmentation, the inner normal direction of the ellipse is used for the second case to determine the split point. However, the normal direction is difficult to be obtained because the equation of the curve is unknown. Therefore, this paper proposes a low-computational Approximate Normal Curvature Field (ANCF) to estimate the inner normal direction and curvature of the curve. Fig. 6 shows a schematic of the calculation of ANCF at a specific sampling point. Once all split points in the first stage are obtained, ANCF is used to split all the split points in the second stage. ANCF is a vector field that is computed as

$$\begin{aligned} \boldsymbol{ANCF}(i) &= \sum_{\Delta \in \mathcal{N}(i)} \boldsymbol{S}(i, \Delta) \\ \boldsymbol{S}(i, \Delta) &= \frac{|\boldsymbol{P}_{i-\Delta}\boldsymbol{P}_{i+\Delta} \times \boldsymbol{P}_{i-\Delta}\boldsymbol{P}_i|}{|\boldsymbol{P}_{i-\Delta}\boldsymbol{P}_{i+\Delta}|^2} \omega_\Delta(\boldsymbol{n}_\perp)_\Delta \end{aligned} \tag{7}$$

where P_i is the position of the i-th sampling point, Δ is the bias on both sides of the i-th sampling point, ω is a flip Gaussian function that increases as Δ increases to counteract the effects of noise from small bias and $\boldsymbol{n}_\perp$ is the unit vector perpendicular to $\boldsymbol{P}_{i-\Delta}\boldsymbol{P}_{i+\Delta}$. Fig. 1(e) shows the ANCF in the real scenario. Since the ANCF only reflects the inner normal vector of a single edge on the checkerboard-like marker, we collected one set of edge sampling points from the real scenario in Fig. 1 and made it more complex by flipping, splicing, and extending sampling points to it to test

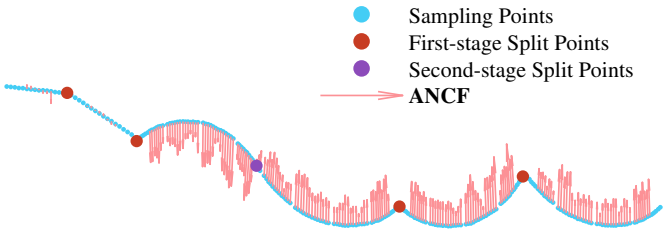

Fig. 7. The result of the segmentation of a set of sampling points. Blue dots are flipped, spliced, and extended from the sampling points obtained in the real scenario. Red dots represent all the split points picked out in the first stage, while purple point represents the split points selected in the second stage using ANCF.

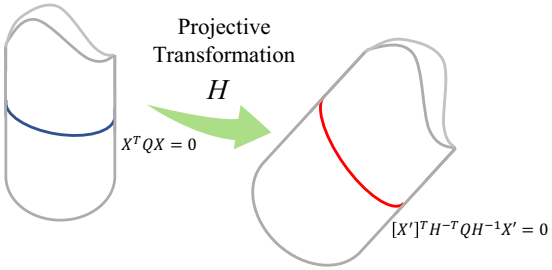

Fig. 8. Schematic diagram of quadratic form remaining non-degenerate under projective transformation. Blue curve and red curve are at the same location on the cylinder.

the segmentation capability of the ANCF. Fig. 7 shows the ANCF schematic of this edge. As can be seen, this method has obtained a good segmentation performance under sophisticated situations.

F. Subpixel Extraction Based on Ellipse Fitting

After obtaining interval points in each curve, for each segment of discrete points, the least-squares method is used to fit an elliptical curve to it. With the generation of some elliptic curves, the intersections of all curves are found, and some of the reasonable intersections are considered to be the accurate corner locations with subpixel accuracy. The ellipse fitting procedure is described in detail below.

Therefore, these edges are the quadratic form of Euclidean space $\mathbb{R}^3$. After the perspective projection transformation by the camera, they are transformed into the quadratic form $\mathscr{F}$ of Image space $\mathbb{R}^2$

$$\mathscr{F} : \alpha x^2 + \beta xy + \gamma y^2 + \delta x + \epsilon y + \zeta = 0 \tag{8}$$

The above formula can be expressed as a matrix form

$$\begin{aligned} &\mathscr{F} : \mathbf{X}^{\mathrm{T}}\mathbf{Q}\mathbf{X} = 0 \\ &\mathbf{Q} = \begin{pmatrix} \alpha & \beta/2 & \delta/2 \\ \beta/2 & \gamma & \epsilon/2 \\ \delta/2 & \epsilon/2 & \zeta/2 \end{pmatrix} \end{aligned} \tag{9}$$

In addition, the non-degenerate property of the quadratic form under the projective transformation provides strong support for our method as Fig. 8 shown. Consider the change of a quadratic form under the projective transformation $\mathbf{H}$, which means the point transformation $x' = \mathbf{H}x$

Fig. 9. Schematic diagram of subpixel corner extraction. The position of a corner is the intersection of two ellipses fitted by edges.

$$\mathscr{F} : \mathbf{X}^{\mathrm{T}}\mathbf{Q}\mathbf{X} = (\mathbf{X}')^{\mathrm{T}}[\mathbf{H}^{-1}]^{\mathrm{T}}\mathbf{Q}\mathbf{H}^{-1}\mathbf{X}' = 0 \tag{10}$$

Here, a numerical direct least-squares fitting method proposed by Fitzgibbon [27] as well as Halíř and Flusser [28] is introduced. In this method, the error function constraint is constructed by the least square method, and the elliptical quadratic coefficient matrix is divided into blocks according to the characteristics of the matrix, which is divided into quadratic parts and linear parts for fitting. The method is strongly robust to noise and only needs a fraction of the sample points on the ellipse to fit. Fig. 9 illustrates the elliptical quadratic fitting performance of each curve.

Finally, it is intuitive that the exact corner position is considered as the intersection of two curves (or lines) corresponding to the two corner edges, thanks to the significant fitting performance of the edges. To improve the robustness and stability of the method, an analytical solution based on a cubic equation is given to solve the intersection of two conic curves. [29] Let C_1 and C_2 be two matrices of the conics $\mathscr{C}_1$ and $\mathscr{C}_2$, we set a pencil of conics $\{\lambda C_1 + \mu C_2 \mid \lambda, \mu \in \mathbb{R}\}$ which pass through the same four real intersections as the two conics. Next, the proper λ and μ are searched to find a suitable degenerate matrix by calculating

$$\det(\lambda C_1 + \mu C_2) = 0. \tag{11}$$

Here, it is known by theoretical analysis that there exists at least one non-zero result in λ or μ, which leads to a corresponding degenerate conic. Let $C = \lambda C_1 + \mu C_2$, this degenerate conic can be split into two lines. All that remains is to use the cubic equation to solve for the intersection of each line with any of the conic $\mathscr{C}_1$ or $\mathscr{C}_2$ to get all the intersections of the two conics. Using the previously obtained corner position at the pixel level, the closest of the two or four resulting intersections is kept as the subpixel corner position.

IV. Experiments and Analyses

This section gives evaluations of the proposed method, including localization accuracy using synthetic corner, triangulation reprojection errors on stereo images, and pose estimation on a curved object, which can reflect the accuracy and robustness of our method. Experimental conditions were as follows. The cameras used were HikVision MV-CA023-10GM industrial cameras (monochrome, 1920×1200 pixels). The computer was equipped with Intel I7-11700K (2.50 GHz).

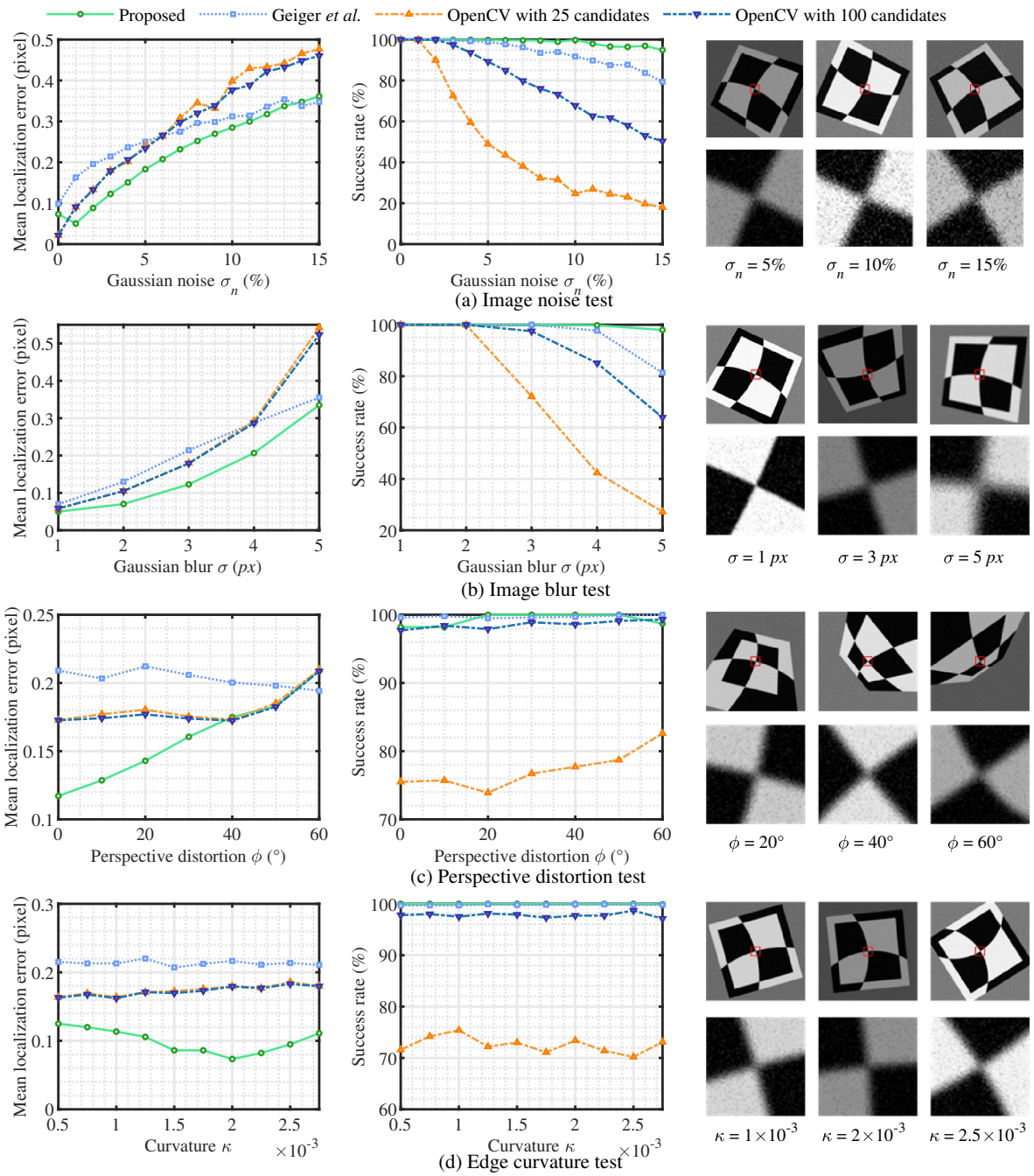

Fig. 10. Analysis of the influence of noise, blur, and edge curvature on the localization precision of some reference methods and the proposed method.

The checkerboard-like markers were printed on a PVC sticker (220×220 mm) with 10 columns and rows. To prevent ink bleeding on checkerboard-like markers, we recommend using the PVC stickers, which are less affected by ink bleeding, to print the pattern. The size of the neighborhood window of each corner in our method was $n = 7$. Also, the hyperparameters for our method were set as follows: $n_{nms} = 3$, $\tau_{nms} = 2$, $\theta^*_{edge} = 15°$, $w = h = 15$, and $T_{correlation} = 0.25$.

A. Synthetic Corner Localization Evaluation

Firstly, a large number of synthetic corners under different circumstances were created to evaluate the corner localization precision of our method with some reference corner detection methods. Here, we use two reference methods, the first one is Geiger's method [17], and the second one uses the function *goodFeaturesToTrack* [24] in OpenCV as the corner detector and uses the function *cornerSubPix* [21] in OpenCV as the subpixel refinement method. Besides, the function *goodFeaturesToTrack* in OpenCV requires the number of corners as input. Due to its low success rate of corner detection, we tested

this method with two different inputs, 25 candidates and 100 candidates. To facilitate the experimental evaluation, the exact subpixel corner positions of the synthesized images were set in advance. As shown in Fig. 10, corners were taken from the neighborhood centered on the intersection of two larger circles whose curvature can be easily adjusted through their radii. Out-of-focus blur (σ), imaging noise (σ_n), low lighting (In), random perspective distortion (ϕ), and edge curvature (κ) were evaluated in four tests. Here, low lightning (In) is defined as the maximum brightness of the image, and random perspective distortion (ϕ) is defined as the out-of-plane rotation angle.

1) *Image noise test:* Each image was applied with a Gaussian noise $\sigma_n \in (0, 15)\%$, a fixed blur $\sigma = 3\ px$, a random maximum image intensity $In \in (0.5, 1)$, a random edge curvature $\kappa \in (1 \times 10^{-3}, 1.5 \times 10^{-3})$, and a random $\phi \in (0, 15)^\circ$.
2) *Image blur test:* Each image was applied with a blur $\sigma \in (1, 5)\ px$, a fixed Gaussian noise $\sigma_n = 3.0\%$, a random maximum image intensity $In \in (0.5, 1)$, a random edge curvature $\kappa \in (1 \times 10^{-3}, 1.5 \times 10^{-3})$, and a random $\phi \in (0, 15)^\circ$.
3) *Perspective distortion test:* Each image was generated with an out-of-plane rotation angle $\phi \in (0, 60)^\circ$, a fixed Gaussian noise $\sigma_n = 3.0\%$, a fixed blur $\sigma = 3\ px$, a random maximum image intensity $In \in (0.5, 1)$, and a random edge curvature $\kappa \in (1 \times 10^{-3}, 1.5 \times 10^{-3})$.
4) *Edge curvature test:* Each image was generated with an edge curvature $\kappa \in (5 \times 10^{-4}, 3 \times 10^{-3})$, a fixed Gaussian noise $\sigma_n = 3.0\%$, a fixed blur $\sigma = 3\ px$, a random maximum image intensity $In \in (0.5, 1)$, and a random $\phi \in (0, 15)^\circ$.

For each test, the image synthesis and localization process were repeated by 1000 runs to obtain statistically meaningful results. A 640×640 pixel image was generated with an in-plane rotation angle randomly sampled from $(0, 2\pi)$. The ground-truth position χ^*_{gt} of every synthetic image was set to be the center pixel with a random offset of the true subpixel position by ±0.5 pixels horizontally and vertically. The mean localization error (MLE) $|\chi^* - \chi^*_{gt}|$ between the localization result χ^* and the ground-truth position was calculated as the indicator of localization accuracy. Furthermore, localization errors from all 1000 images were averaged as the result errors for different situations.

Evaluation results are illustrated in Fig. 10. Image noise is ubiquitous and frequently becomes the most direct cause of localization errors, which can significantly influence the fitting model. The performance of all methods in the image noise test is clearly reduced with increasing noise. Compared with the OpenCV method, the proposed method achieved a performance improvement of no less than 18.75% in all tests. As for Geiger's method, the accuracy of the proposed method is significantly higher than it is under low noise, but the gap of positioning error is gradually decreasing as the noise increases.

For cameras with traditional fixed focal length lenses, image blur is common and unavoidable when the target object moves in a large range, which can significantly influence the localization accuracy. When $\sigma = 0$ (which is impossible in reality), the OpenCV method received the best result due to its iterative optimization method, while it was difficult for our method to extract the precise edge position of this ideal edge model, which led to an abnormal rise in the experiment result. As σ increases from 1, the proposed method exhibited better performance. Specifically, the evaluation result showed an over 35.98% performance improvement with the OpenCV method at $\sigma = 5$ and a 46.04% performance improvement with Geiger's method at $\sigma = 2$.

Fig. 11. Experimental setup for evaluation of the detection accuracy. A 3D printed model with a PVC marker attached on is placed in front of a stereovision system. The image pairs on the right are captured by this system.

The change in viewing angle has a huge impact on the positioning accuracy of the corner detector. A larger out-of-plane rotation angle leads to a decrease in the edge angle as Fig. 10(c) shows, resulting in an increase in the localization uncertainty of the corner. As the edges approach with an increased viewing angle, which makes the edge sampling difficult, the accuracy of our method decreases as the viewing angle increases but remains low compared to the reference methods.

The main difference between planar and curved corners is the curvature of the edges. Theoretically, the reference methods should suffer a localization deviation due to the edge not being completely perpendicular to the gradient direction. Hence, it is necessary to evaluate the effect of edge curvature on corner positioning accuracy. With the increase of edge curvature, the proposed method did not reflect the positive correlation between error and curvature and obtained the minimum error among all testing methods.

At the same time, the proposed method had consistently maintained the highest success rate (SR). A success localization result was defined as $|\chi^* - \chi^*_{gt}| \leq 1$, though the OpenCV method with more candidates did not perform better when the success rate increased significantly. This result verified the robustness of the proposed method in harsh environments.

B. Real-World Stereo Triangulation Evaluation

To further evaluate the real-world positioning accuracy, a triangulation performance experiment was designed using stereo images captured by the two calibrated industrial cameras mentioned above. As shown in Fig. 11, a checkerboard-like marker was attached to a 3D printed model that is designed as a combination of several elliptical columns. It was placed in the common field of view of the stereo camera

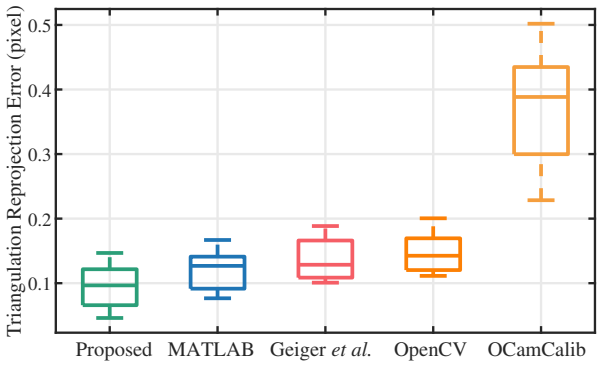

Fig. 12. Evaluations of average triangulation reprojection error of the proposed method with reference methods.

TABLE I
PERFORMANCE COMPARISON OF AVERAGE REPROJECTION ERROR ON STEREO IMAGES WITH INCREASING EDGE CURVATURE AROUND CORNERS

Method	Curvature ($\times 10^{-3}$)						
	Small	Large					
	(0, 1)	(1, 2)	(2, 3)	(3, 4)	(4, 5)	(5, 6)	(6, $+\infty$)
Proposed	0.0856	**0.0611**	**0.0764**	**0.1015**	**0.0904**	**0.1194**	**0.1046**
MATLAB	**0.0565**	0.0655	0.1054	0.1363	0.1310	0.1730	0.2780
Geiger *et al.*	0.0766	0.0899	0.1536	0.1876	0.1818	0.1814	0.1429
OpenCV	0.0673	0.0894	0.1572	0.1956	0.1957	0.1870	0.1611
OCamCalib	0.2306	0.2046	0.1879	0.2447	0.1940	0.2417	0.2911

and 10 pairs of images were collected by changing the model's poses and ambient light. Here, the proposed method is compared with five reference algorithms, Geiger's [17], Duda's [30], OCamCalib [31], OpenCV (using the function *findChessboardCorners* to detect corners with the function *cornerSubPix* for subpixel refinement), and MATLAB (using the function *detectCheckerboardPoints*), respectively. The average reprojection Root Mean Squared Error (RMSE) is calculated as a test metric by extracting the corners of the left and right views of each image pair and obtaining the spatial positions of their corners using triangulation.

The average reprojection error for each method is summarized in Fig. 12. The proposed method achieved the lowest result, which reflected the high precision and robustness of our method. Our method achieved an improvement of more than 18.25% compared to all reference methods, while the method Duda and Frese [30] recently proposed with high localization accuracy was unable to successfully extract corners in these images. The lowest RMSE result demonstrated the best performance of our method in practical applications, such as 3D reconstruction and pose estimation on curved surfaces.

In addition, the relationship between the edge curvature of each corner and the corresponding reprojection error was analyzed. Since the proposed method has good edge fitting performance, the curvature at the intersection of the ellipses can be approximated as the curvature of the edges. As listed in Table I, in the case of small curvature, the proposed method did not maintain the lowest error, while in the cases of large curvature, it consistently maintained the minimum error among all methods. Besides, the mean projection error increases in large curvature compared to small curvature in MATLAB, OpenCV, and Geiger's method. Whereas the proposed method still maintained a relatively smooth error variation, reflecting the low influence of curvature on the reprojection error in our method.

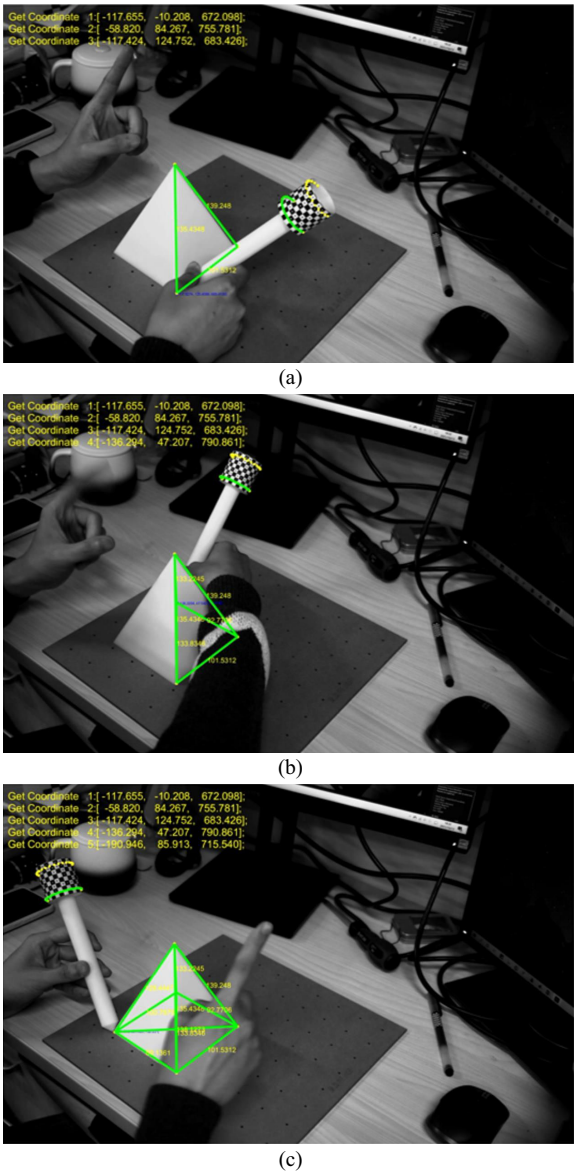

Fig. 13. The pose estimation process for a pen-shaped cylindrical object. The spatial positions of the vertices are obtained by touching each vertex of the square pyramid model with the pen tip, as shown in (a), (b), and (c).

C. Pose Estimation on Curved Object

Due to the limitations of traditional corner detection methods, it is difficult to achieve pose estimation for objects with curved surfaces. By establishing the proposed method, a checkerboard-like marker can be tightly affixed to objects with curved surfaces, thus achieving a stable and high-precision object pose estimation procedure. In this experiment, the HydraMarker [1], a checkerboard-like marker with a high density

[1]https://github.com/Lilin2015/Author---HydraMarker

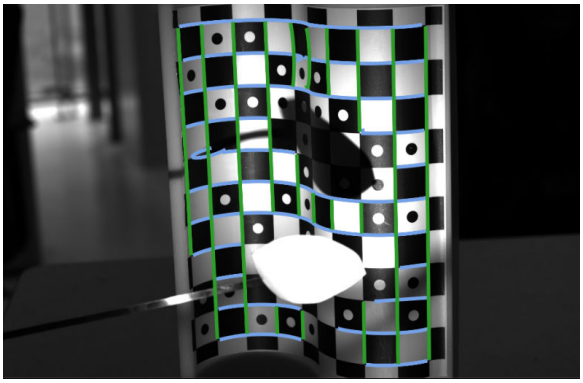

Fig. 14. Schematic diagram of the quadratic fitting results using the proposed method under local illumination changes or occlusion.

of unique features and resistance to bending, was utilized and attached to a pen-shaped cylindrical object for a high-precision pose estimation application. By identifying the corner position of the marker, a PnP (Perspective-n-Point) procedure was used to obtain the pose of the marker and the homogeneous matrix between the pen tip with the marker was acquired to realize the pose tracking of the pen tip. Fig. 13 shows the pose estimation process. It is worth noting that the proposed method is robust to local low-lighting conditions and occlusions as Fig. 14 shows. The failure of partial corner detection in some extreme cases does not affect the quadratic fitting of the remaining corners due to the correct connectivity among these corners, and the accuracy of these corner positions is essentially unaffected.

D. Discussion

According to the results on synthetic corner localization test and real-world triangulation experiment, the proposed method reflects a clear superiority in accuracy and robustness over the compared methods. Compared to the OpenCV method and Geiger's method, which only use information from small neighborhoods around individual corners, the proposed method, which utilizes connectivity and edge information from all corners, shows the best performance against Gaussian noise and blur. However, the reference methods are not affected by the increased curvature of the corner edges due to the small size of corner neighborhoods. For real-world experiments, the proposed method obtains minimal reprojection error on average with small fluctuation, which demonstrates that it can consistently obtain accurate corner positions in different viewing angles and illuminations. However, during the experiments, we found that there may be a slight offset in the segmentation results of the multi-curve segmentation algorithm under different viewpoints. If there is a corner exactly between the offset, it will lead to the same corner belonging to different curve segments under different viewpoints, which often leads to an abnormal increase of reprojection error in triangulation. Nevertheless, existing outlier rejection algorithms such as RANSAC [32] can easily exclude this corner according to the reprojection error, thus not affecting the positioning accuracy. Finally, a demonstration of object pose estimation based on curved markers was given, indicating a promising application of the proposed method.

V. Conclusion and Future Work

In this paper, we have proposed and implemented a precise subpixel corner detection and localization method for checkerboard-like markers on curved surfaces. Firstly, a progressive two-stage corner detector is designed. After that, a Delaunay triangulation procedure is used to organize the connectivity among the corners. Next, the edges of the checkerboard-like marker are fitted by the multi-segment continuous curves based on quadratic form. Finally, the intersection of the corresponding curves is considered the precise corner position. Experiments are carried out to evaluate the performance of the proposed method which demonstrates the best performance of the proposed method in a practical scenario. The feasibility and superiority of the proposed method are demonstrated in the pose estimation test on an object with curved surfaces. The experiments demonstrate that the proposed method can achieve state-of-the-art performance and good feasibility compared to other methods.

In the future, we will extend the proposed method to more complex scenarios with uncertain curvature based on more robust and precise curve segmentation algorithms, and continue to improve the real-time performance of the method.

Acknowledgment

The authors would like to thank Mr. Jie Pan for critical reading and helpful comments on the article preparation.

References

[1] R. Mur-Artal, J. M. M. Montiel, and J. D. Tardos, "ORB-SLAM: A versatile and accurate monocular SLAM system," *IEEE Trans. Robot.*, vol. 31, no. 5, pp. 1147–1163, Oct. 2015.

[2] R. Munoz-Salinas, MJ. Marin-Jimenez, and R. Medina-Carnicer, "SPM-SLAM: Simultaneous localization and mapping with squared planar markers," *Pattern Recognit.*, vol. 86, pp. 156–171, Feb. 2019.

[3] H. Deng, Q. Fu, Q. Quan, K. Yang, and K.-Y. Cai, "Indoor multi-camera-based testbed for 3-D tracking and control of UAVs," *IEEE Trans. Instrum. Meas.*, vol. 69, no. 6, pp. 3139–3156, Jun. 2019.

[4] G. Narita, Y. Watanabe, and M. Ishikawa, "Dynamic projection mapping onto deforming non-rigid surface using deformable dot cluster marker," *IEEE Trans. Vis. Comput. Graphics*, vol. 23, no. 3, pp. 1235–1248, Mar. 2016.

[5] S. Kong, X. Fang, X. Chen, Z. Wu, and J. Yu, "A NSGA-II based calibration algorithm for underwater binocular vision measurement system," *IEEE Trans. Instrum. Meas.*, vol. 69, no. 3, pp. 794–803, Apr. 2019.

[6] M. Calonder, V. Lepetit, C. Strecha, and P. Fua, "Brief: Binary robust independent elementary features," in *Proc. Eur. Conf. Comput. Vis.*, Crete, Greece, Sep. 2010, pp. 778–792.

[7] E. Olson, "AprilTag: A robust and flexible visual fiducial system," in *Proc. IEEE Int. Conf. Robot. Autom.*, Shanghai, China, May 2011, pp. 3400–3407.

[8] B. Atcheson, F. Heide, and W. Heidrich, "CALTag: High precision fiducial markers for camera calibration," in *Proc. Int. Workshop Vis., Model. Vis.*, Siegen, Germany, Nov. 2010, pp. 41–48.

[9] Z. Xing, J. Yu, and Y. Ma, "A new calibration technique for multi-camera systems of limited overlapping field-of-views," in *Proc. IEEE/RSJ Int. Conf. Intell. Rob. Syst.*, Vancouver, Canada, Sep. 2017, pp. 5892–5899.

[10] D. Yang, B. He, M. Zhu, and J. Liu, "An extrinsic calibration method with closed-form solution for underwater opti-acoustic imaging system," *IEEE Trans. Instrum. Meas.*, vol. 69, no. 9, pp. 6828–6842, Feb. 2020.

[11] C. Harris and M. Stephens, "A combined corner and edge detector," in *Proc. Alvey Vis. Conf.*, Manchester, UK, Aug. 1988, pp. 147–151.

[12] S. Bennett and J. Lasenby, "ChESS–Quick and robust detection of chess-board features," *Comput. Vis. and Image Understanding*, vol. 118, pp. 197–210, Jan. 2014.

[13] E. Rosten, R. Porter, and T. Drummond, "Faster and better: A machine learning approach to corner detection," *IEEE Trans. Pattern Anal. Mach. Intell.*, vol. 32, no. 1, pp. 105–119, Nov. 2008.

[14] Q. Zhang and C. Xiong, "A new chessboard corner detection algorithm with simple thresholding," in *Proc. Int. Conf. Intell. Robot. Appl.*, Wuhan, China, Aug. 2017, pp. 532–542.

[15] W. Sun, X. Yang, S. Xiao, and W. Hu, "Robust checkerboard recognition for efficient nonplanar geometry registration in projector-camera systems," in *Proc. ACM/IEEE Int. Workshop Projector Camera Syst.*, Marina del Rey, USA, Aug. 2008, no. 2, pp. 1–7.

[16] Y. Yan, P. Yang, L. Yan, J. Wan, Y. Sun, and K. Tansey, "Automatic checkerboard detection for camera calibration using self-correlation," *J. Electron. Imaging*, vol. 27, no. 3, pp. 1–35, May 2018.

[17] A. Geiger, F. Moosmann, O. Car, and B. Schuster, "Automatic camera and range sensor calibration using a single shot," in *Proc. IEEE Int. Conf. Robot. Autom.*, St Paul, USA, May 2012, pp. 3936–3943.

[18] L. Lucchese and S. Mitra, "Using saddle points for subpixel feature detection in camera calibration targets," in *Proc. IEEE Asia Pac. Conf. Circuits Syst.*, Bali, Indonesia, Dec. 2002, pp. 191–195.

[19] H. Ha, M. Perdoch, H. Alismail, I. So Kweon, and Y. Sheikh, "Deltille grids for geometric camera calibration," in *Proc. IEEE Int. Conf. Comput. Vis.*, Venice, Italy, Oct. 2017, pp. 5344–5352.

[20] S. Placht, P. Fürsattel, E. A. Mengue, H. Hofmann, C. Schaller, M. Balda, and E. Angelopoulou, "Rochade: Robust checkerboard advanced detection for camera calibration," in *Proc. Eur. Conf. Comput. Vis.*, Zurich, Switzerland, Dec. 2014, pp. 766–779.

[21] W. Förstner and E. Gülch. "A fast operator for detection and precise location of distinct points, corners and centres of circular features," in *Proc. ISPRS Intercommission Conf. Fast Process. Photogrammetric Data*, Interlaken, Switzerland, Jun. 1987, pp. 281–305.

[22] D. Chen and G. Zhang, "A new sub-pixel detector for x-corners in camera calibration targets," in *Proc. Int. Conf. Comput. Graph., Vis. Comput. Vis.*, Plzen, Czech, Jan. 2005, pp. 97–100.

[23] A. Datta, J.-S. Kim, and T. Kanade, "Accurate camera calibration using iterative refinement of control points," in *Proc. IEEE Int. Conf. Comput. Vis. Workshops*, Kyoto, Japan, Sep. 2009, pp. 1201–1208.

[24] J. Shi and Tomasi, "Good features to track," in *Proc. IEEE Conf. Comput. Vis. Pattern Recognit.*, Seattle, USA, Jun. 1994, pp. 593–600.

[25] R. M. Haralick, L. T. Watson, and T. J. Laffey, "The topographic primal sketch," *Int. J. Robot. Res.*, vol. 2, no. 1, pp. 50–72, Mar. 1983.

[26] A. Neubeck and L. Van Gool, "Efficient Non-Maximum Suppression," in *Proc. Int. Conf. Pattern Recognit.*, Hong Kong, China, Aug. 2006, pp. 850–855.

[27] A. Fitzgibbon, M. Pilu, and R. B. Fisher, "Direct least square fitting of ellipses," *IEEE Trans. Pattern Anal. Mach. Intell.*, vol. 27, no. 5, pp. 476–480, May 1999.

[28] R. Halíř and J. Flusser, "Numerically stable direct least squares fitting of ellipses," in *Proc. Int. Conf. Comput. Graph. Visualization*, Plzen, Czech, Feb. 1998, pp. 125–132.

[29] J. Richter-Gebert, *Perspectives on Projective Geometry: A Guided Tour Through Real and Complex Geometry*. Heidelberg, Germany: Springer, 2011, pp. 194–199.

[30] A. Duda and U. Frese, "Accurate detection and localization of checkerboard corners for calibration," in *Proc. British Mach. Vis. Conf.*, Newcastle, UK, Sep. 2018, pp. 1–10.

[31] D. Scaramuzza, A. Martinelli, and R. Siegwart, "A toolbox for easily calibrating omnidirectional cameras," in *Proc. IEEE/RSJ Int. Conf. Intell. Robot. Syst.*, Beijing, China, Oct. 2007, pp. 5695–5701.

[32] M. A. Fischler and R. Bolles, "Random sample consensus: A paradigm for model fitting with applications to image analysis and automated cartography," *Commun. ACM*, vol. 24, no. 6, pp. 381–395, Jun. 1981.

Shaoan Wang received the B.E. degree in mechanical engineering from the School of Mechatronical Engineering, Beijing Institute of Technology, Beijing, China, in 2021. He is currently pursuing the Ph.D. degree in general mechanics and foundation of mechanics with the College of Engineering, Peking University, Beijing, China. His current research interests include robot vision and visual localization.

Mingzhu Zhu received the B.E, M.E, and D.E. degrees in the School of Mechanical Engineering and Automation, Fuzhou University, Fuzhou, China, in 2012, 2015, and 2019, respectively. From 2019 to 2021, he was a Postdoctoral Research Fellow with BIC-ESAT, College of Engineering, Peking University, Beijing, China. In 2021, he joined Fuzhou University, as an Associate Scientist. His current research interests include computer vision and image processing.

Yaoqing Hu received the B.E. degree from University of Science and Technology Beijing, China, in 2018, and the M.E. degree from University of Science and Technology Beijing, China, in 2021. He is currently pursuing the Ph.D. degree in general mechanics and foundation of mechanics with the College of Engineering, Peking University, Beijing, China. His research interests include computer vision and robotics.

Dongyue Li received the B.E. degree from the School of Aerospace, Beijing Institute of Technology, Beijing, China, in 2020. He is currently pursuing the Ph.D. degree in general mechanics and foundation of mechanics with the College of Engineering, Peking University, Beijing, China. His current research interests include robot vision and surgical robot.

Fusong Yuan received the B.A. degree in Dentistry from Weifang Medical University, Shandong, China, in 2008, and the M.E. degree and Ph.D. degree in Prosthodontics from Peking University, Beijing, China, in 2011 and 2014, respectively.

In 2014, he joined the Peking university school and hospital of Stomatology, as a dentist, teacher, and researcher. In 2021, he was promoted to associate chief physician. His current research interest includes the application research of robotic and femtosecond laser technology in stomatology.

Junzhi Yu (Fellow, IEEE) received the B.E. degree in safety engineering and the M.E. degree in precision instruments and mechanology from the North University of China, Taiyuan, China, in 1998 and 2001, respectively, and the Ph.D. degree in control theory and control engineering from the Institute of Automation, Chinese Academy of Sciences, Beijing, China, in 2003.

From 2004 to 2006, he was a Postdoctoral Research Fellow with the Center for Systems and Control, Peking University, Beijing. In 2006, he was an Associate Professor with the Institute of Automation, Chinese Academy of Sciences, where he became a Full Professor in 2012. In 2018, he joined the College of Engineering, Peking University, as a Tenured Full Professor. His current research interests include intelligent robots, motion control, and intelligent mechatronic systems.